SUITOR: selecting the number of mutational signatures through cross-validation

Donghyuk Lee[1], Difei Wang[2], Xiaohong R. Yang[2], Jianxin Shi[2], Maria Teresa Landi[2], Bin Zhu[2,#]

[1]Department of Statistics, Pusan National University, Busan, Korea

[2]Division of Cancer Epidemiology and Genetics, National Cancer Institute, National Institutes of Health, Bethesda, MD, USA

To whom correspondence should be addressed to: bin.zhu@nih.gov

Abstract

For *de novo* mutational signature analysis, the critical first step is to decide how many signatures should be expected in a cancer genomics study. An incorrect number could mislead downstream analyses. Here we present SUITOR (Selecting the nUmber of mutatIonal signaTures thrOugh cRoss-validation), an unsupervised cross-validation method that requires little assumptions and no numerical approximations to select the optimal number of signatures without overfitting the data. *In vitro* studies and *in silico* simulations demonstrated that SUITOR can correctly identify signatures, some of which were missed by other widely used methods. Applied to 2,540 whole-genome sequenced tumors across 22 cancer types, SUITOR selected signatures with the smallest prediction errors and almost all signatures of breast cancer selected by SUITOR were validated in an independent breast cancer study. SUITOR is a powerful tool to select the optimal number of mutational signatures, facilitating downstream analyses with etiological or therapeutic importance.

Background

Mutational signatures are patterns of somatic mutations imprinted on the cancer genome by operative mutational processes. At least 49 single base substitution mutational signatures have been identified across cancer types[1], with some associated with exogenous mutagenic exposures[2-4] and endogenous mutational processes[5-8]. Moreover, mutational signatures have been proposed to identify cancer predisposition genes (e.g., *NTHL1* in breast cancer[9]), and to stratify cancer patients[10-13] for precision treatment. In these studies, deciding the expected number of signatures is the pivotal first step, which determines the downstream steps of extracting signature profiles, estimating signature contributions and stratifying tumors based on signatures for treatment. As an example, the Pan-Cancer Analysis of Whole Genomes (PCAWG) consortium reported that the discordance between the extracted and known signatures is usually caused by the difficulty in selecting the correct number of signatures[1].

Despite the many algorithms proposed to extract signature profiles[14-18] and estimate signature contributions[19,20], relatively little emphasis has been placed on selecting the correct number of *de novo* mutational signatures in cancer genomics studies[21,22]. SomaticSignatures[14] chooses the number of signatures based on the residual sum of squares and the explained variance without a clearly defined selection criterion. SigProfiler[15] considers the mean reconstruction error and the stability of signature extraction; however, it is unclear how these features could be combined to jointly predict the number of signatures. EMu[16] and signeR[17] adopt a Bayesian information criterion (BIC)[23]. Although BIC is a popular model selection criterion for supervised learning (e.g., regression and classification) where the number of parameters is fixed, it may not

be applicable to unsupervised learning, including mutational signature analysis, where the number of parameters increases with the sample size (other limitations of BIC elaborated in Supplementary Note 1). SignatureAnalyzer[1] uses an automatic relevance determination (ARD) prior[24] which imposes a sparsity assumption on mutation profiles and contributions. The number of signatures chosen by signatureAnalyzer is sensitive to the pre-specified sparsity assumption, especially hyperparameters of the ARD prior and the tolerance level.

To overcome the limitations of previous methods, we propose selecting the number of signatures through cross-validation. Selecting the number of signatures is essentially a problem of model selection, which has been addressed by cross-validation in other research areas[25,26], including identification of cancer subtypes[27], exploration of population structure[28] and prediction of lymph node metastasis[29]. In the setting of mutational signature analysis, cross-validation splits the full dataset (here, the mutation counts) into a training set and a validation set; for a given number of signatures, these signatures are estimated in the training set and then they are used to predict the mutations in the validation set. Multiple candidate numbers of signatures are considered; and the number of signatures which predicts most closely the mutations in the validation (not the training) set is selected. Hence, cross-validation can prevent selecting too few or too many signatures (corresponding to an underfitting or overfitting model), both of which would predict mutation counts in the validation set poorly. In addition, unlike the BIC or the ARD prior, cross-validation requires little assumptions and no numerical approximations[26]. Therefore, cross-validation provides a viable solution for selecting the correct number of signatures.

Despite being conceptually appealing, the standard cross-validation approach does not work for unsupervised mutational signature analysis. In the standard cross-validation scheme, it is feasible to remove a subset of subjects all together as a validation set because parameters (e.g., regression coefficients) are identical across subjects. However, mutation contributions in mutational signature analysis are tumor-specific parameters. If mutation counts of a subset of tumors were removed all together as a validation set, these counts would be used twice (for estimating tumor-specific mutation contributions and calculating the prediction error), which would underestimate the prediction error. Instead, cross-validation for mutational signature analysis requires retaining all tumors in the training set but removing some mutation counts from each tumor as a validation set. Consequently, missing data emerge in the training set, which would cause current methods for mutational signature analysis to fail.

These limitations are overcome by SUITOR (Selecting the nUmber of mutatIonal signaTures thrOugh cRoss-validation), an unsupervised cross-validation method that selects the optimal number of signatures to attain the minimal prediction error in the validation set. SUITOR extends the probabilistic model to allow missing data in the training set, which makes cross-validation feasible. Moreover, we propose an expectation/conditional maximization (ECM) algorithm[30] to extract signature profiles, estimate mutation contributions and impute the missing data simultaneously. We demonstrated SUITOR's superior performance using *in vitro* experimental data, *in silico* simulations, *in vivo* applications to 2,540 tumors across 22 cancer types, and validation of signatures of breast cancer in additional 440 breast tumors.

Results

Overview of SUITOR

Mutational signature analysis decomposes the catalog matrix of somatic mutations. Take single base substitution (SBS) as an example. A mutation catalog matrix $\mathbf{V}$ of size $\mathrm{N} \times 96$ contains mutation counts for N cancer genomes and 96 SBS catalogs. Each SBS catalog refers to a mutated pyrimidine (C or T) in the center and two unmutated adjacent nucleotides (flanking 5' and 3' bases) with total $4 \times 6 \times 4 = 96$ catalogs. For example, a genomic sequence A<u>C</u>G in the normal tissue is mutated to A<u>G</u>G in the tumor tissue. This SBS belongs to the A[C > G]G mutation catalog.

SUITOR is built upon a probabilistic model[31,32], for which the maximum likelihood estimation (MLE) is equivalent to the solution of non-negative matrix factorization (NMF), the most popular method for mutational signature analysis[15]. Given the number of signatures r to be extracted, NMF factorizes the mutation catalog matrix into two non-negative matrices: signature contribution matrix $\mathbf{W}$ of size $\mathrm{N} \times r$ and signature profile matrix $\mathbf{H}$ of size $r \times 96$ such that $\mathbf{V} \approx \mathbf{WH}$. Each row of $\mathbf{W}$ contains attributions of r signatures, reflecting how intense r mutational signatures are in a tumor; each row of $\mathbf{H}$ forms a signature profile with the elements summed to 1, showing how 96 mutation catalogs comprise a signature profile. To estimate $\mathbf{W}$ and $\mathbf{H}$, it is common to minimize the generalized Kullback-Leibler (KL) divergence

$$D_{KL}(\mathbf{V} \mid \mathbf{WH}) = \sum_{p=1}^{96} \sum_{n=1}^{N} \left\{ v_{np} \log \left(v_{np} \Big/ \sum_{j=1}^{r} w_{nj} h_{jp} \right) + \sum_{j=1}^{r} w_{nj} h_{jp} - v_{np} \right\},$$

subject to $w_{nj} \geq 0$ and $h_{jp} \geq 0$ with $1 \leq j \leq \mathrm{r}$, $1 \leq n \leq \mathrm{N}$ and $1 \leq p \leq 96$. Lowercase letters, v_{np}, w_{nj} and h_{jp}, denote elements of the corresponding matrices, $\mathbf{V}$, $\mathbf{W}$ and $\mathbf{H}$, respectively. NMF can also be solved with other objective functions such as Frobenius norm or more general β-divergence, depending on the applications[24].

Notably, minimization of the generalized KL divergence is equivalent to maximize a likelihood function of a probabilistic NMF model[32,33]. Indeed, for a Poisson NMF model, v_{np} of the nth tumor and pth mutation catalog is assumed to be independently distributed, following a Poisson distribution with mean $\sum_{j=1}^{r} w_{nj} h_{jp}$. The log-likelihood of Poisson NMF model can be written as $\log\{\Pr(\mathbf{V} \mid \mathbf{WH})\} = -D_{KL}(\mathbf{V} \mid \mathbf{WH}) + C$ with a constant C. Therefore, minimizing generalized KL divergence $D_{KL}(\mathbf{V} \mid \mathbf{WH})$ is equivalent to maximizing the log-likelihood $\log\{\Pr(\mathbf{V} \mid \mathbf{WH})\}$. In addition, it could been shown that the multiplicative update algorithm[34], which is commonly used to minimize the generalized KL divergence, is equivalent to an expectation/conditional maximization (ECM) algorithm[30] for the Poisson NMF model (Supplementary Note 2). These two equivalences are used to develop SUITOR.

As mentioned above, NMF or equivalently the Poisson NMF model requires a given number of signatures r, which is unknown in practice; and SUITOR can select this number empirically. The steps of SUITOR are outlined as follows (with a schematic illustration in Fig.1): 1) the mutation catalog matrix is separated into the training and validation sets. The training set contains missing data held out as validation data; 2) the missing data are imputed in the initial step; 3) the ECM algorithm iteratively imputes the missing data in the expectation step (E-step) and estimates the signature contributions (of the **W** matrix) and profiles (of the **H** matrix) in the

conditional maximization steps (CM-steps) until the ECM algorithm allows $\mathbf{V} \approx \mathbf{WH}$ for a given number of signatures; 4) the missing data are imputed and compared to the validation data to calculate the prediction error in the validation set; 5) The above described steps are conducted for multiple candidate numbers of signatures and the one with the minimal prediction error will be chosen as the optimal number of signatures (corresponding to the red dot in the prediction error curve of validation set in Fig. 1).

There are three key contributions of SUITOR. First, SUITOR selects the number of signatures with the minimal prediction error, which prevents selecting too few or too many signatures (as model underfitting or overfitting). Although the prediction error in the training set is reduced with increasing signatures (as illustrated by the prediction error curve of the training set in Fig. 1), the prediction error in the validation set will decrease first (due to the model underfitting with insufficient signatures) and then inflate (due to the model overfitting with redundant signatures). This is the well-known bias-variance tradeoff for model complexity[35] measured by the number of signatures in the setting of mutational signature analysis. Second, the cross-validation scheme of SUITOR guarantees that the missing data pattern does not depend on the remaining or missing mutation counts in the training set. Hence, the missing data mechanism is missing completely at random (MCAR), which ensures that the estimated signature profiles and contributions would not be biased due to the missing data[36]. Third, the proposed ECM algorithm for SUITOR enjoys the convergence property, which guarantees the increase of the likelihood function over iterations until the ECM algorithm converges[30].

158 **Evaluation of SUITOR in two *in vitro* studies**

159 We assessed the performance of SUITOR in two experimental studies[2,5], for which the true
160 number and profile of signatures were generated experimentally and validated *in vitro* (see
161 details in Methods). The first study created endogenous mutational signatures through CRISPR-
162 Cas9-mediated knockouts of DNA repair genes in an isogenic human cell line[5]. The second study
163 generated exogenous mutational signatures in human-induced pluripotent stem cell (iPSC) lines
164 exposed to environmental or therapeutic mutagens[2]. For both studies, we evaluated whether
165 SUITOR could correctly select the number of signatures and recover the profiles of single base
166 substitution signatures. We then compared SUITOR's performance with sigProfiler,
167 signatureAnalyzer and signeR.

168

169 For the *in vitro* CRISPR-Cas9-mediated knockout study of the DNA repair gene *MSH6,* SUITOR
170 correctly detected the background signature, which existed before the knockout of *MSH6* and
171 *MSH6* knockout-induced signature (Fig. 2a) and recovered the corresponding signature profiles
172 (Fig. 2b; Supplementary Table 1). SigProfiler, signatureAnalyzer and signeR correctly identified
173 these two signatures as well (Supplementary Fig. 1; Supplementary Table 1). Next, we extracted
174 signatures of knockout studies of six DNA repair genes (*CHEK2*, *NEIL1*, *NUDT1*, *POLB*, *POLE* and
175 *POLM)*, which did not induce experimentally detectable signatures[5]. SUITOR and the other
176 three methods correctly identified one background signature only without false detection of
177 knockout-induced signatures (Supplementary Fig. 2). We conclude that in this *in vitro* study
178 with at most two signatures, all four methods perform equally well. This is not the case when
179 the number of signatures increases as shown below.

180 For the *in vitro* study of 79 exogenous mutagens, stable mutational signatures were
181 experimentally identified for 28 mutagens. These 28 signatures are not distinct as some
182 signatures are very similar to each other (e.g., benzo[a]pyrene (BaP) and benzo[a]pyrene-7,8-
183 dihydrodiol-9,10-epoxide (BPDE), both of which are polycyclic aromatic hydrocarbons (PAHs),
184 mutagens of tobacco smoke; Supplementary Fig. 3). Although all four methods could find the
185 background mutational signature, SUITOR detected 9 additional signatures induced by
186 mutagens (Figure 2c, 10 signatures, including one background signature and 9 mutagen-
187 induced signatures), sigProfiler detected 4, signatureAnalyzer 8, and signeR 5 additional
188 signatures (Figure 2d; Supplementary Fig. 4; Supplementary Table 2); the signature of 1,2-
189 dimethylhydrazine (1,2-DMH) was detected by SUITOR and missed by the other methods.
190 Besides detecting more true signatures, SUITOR also achieved the lowest prediction error
191 (SUITOR:1292.5; sigProfiler:2295.4; signatureAnalyzer:2176.6; signeR:1585.1). This indicates
192 that the signatures detected by SUITOR in the training set predicted most closely the mutation
193 counts in the validation set. When we stratified the tumor subclones based on the signatures
194 detected by at least one method, SUITOR and signatureAnalyzer were able to separate most
195 subclones into distinct clusters, each corresponding to a unique mutagen exposure
196 (Supplementary Fig. 5). In contrast, SigProfiler merged subclones exposed to BPDE and
197 dibenz[a,h]anthracene diol-epoxide (DBADE); signeR mixed subclones exposed to N-ethyl-N-
198 nitrosourea (ENU) and 1,2-DMH; and both SigProfiler and signeR mixed subclones exposed to
199 9-Nitrochrysense and aristolochic acid I (AAI).
200
201 We note that *in vitro* study of exogenous mutagens favors the method of signatureAnalyzer.
202 SignatureAnalyzer implicitly assumes few signatures are present per sample and hence the

203 loadings of signatures are sparse, which holds here since each sample was treated with a single
204 mutagen in this *in vitro* study of exogenous mutagens. In spite of that, SUITOR performed better
205 than signatureAnalyzer. When the sparsity assumption does not hold, as demonstrated in *in silico*
206 simulations and the PCAWG study described below, signatureAnalyzer would find more false-
207 positive signatures than the other methods. In contrast, SUITOR, which does not rely on the
208 sparsity assumption, is not susceptible to it.
209
210 ***In silico* simulation studies**
211 We evaluated SUITOR and three other methods through additional *in silico* simulations. First,
212 we evaluated the scenario when only random mutations occur. SUITOR identified one random
213 signature in 20 of 20 replicates while other methods found many more signatures (as many as
214 96 signatures for signatureAnalyzer; Supplementary Table 3). Note that the random signature
215 identified by SUITOR is similar to SBS3 (cosine similarity = 0.87), implying that SBS3 would
216 possibly be caused by random mutations. Next, we considered a setting of one true signature,
217 for which any additional signature found would be a false positive (details in Methods). SUITOR,
218 sigProfiler and signeR correctly identified the single true signature (Supplementary Fig. 6) in 20
219 of 20 replicates; signatureAnalyzer found a false positive signature (Fig. 3a) in 17 of 20
220 replicates. Finally, we examined a setting of nine true signatures with varying signature
221 contributions (details in Methods; Supplementary Fig. 7; Supplementary Table 4). All methods
222 correctly identified six common signatures (SBS1, 2, 3, 5, 13, 18) in 20 of 20 replicates; SUITOR
223 and signatureAnalyzer detected two rare signatures (SBS8,41) in more replicates than the other
224 two methods (Fig. 3b). None of the methods identified the extremely rare and flat signature

225 SBS40 (present in one tumor only). Notably, all methods detected no other signatures besides
226 the nine true signatures. Together, the simulation studies suggest that SUITOR is able to find
227 both common and rare signatures while well controlling the rate of false positives.
228
229 **Detection of pan-cancer mutational signatures**
230 We tested the four methods in whole-genome sequencing (WGS) data of 2,540 tumors across
231 22 cancer types from the Pan-Cancer Analysis of Whole Genomes (PCAWG) study[1] (details in
232 Methods).
233
234 First, we extracted *de novo* mutation signatures one cancer type at a time for eight cancer
235 types, each with at least 100 tumors. Unlike in *in vitro* or *in silico* studies, the true signatures
236 were unknown here. Nevertheless, we could evaluate if the signatures detected in part of the
237 dataset predict mutation counts in the remaining part well. Specifically, the mutation catalog
238 matrix is separated into training, validation and testing sets, the last of which is used to
239 evaluate the performance of the selected number of signatures (details in Methods). Among
240 the four methods, SUITOR clearly attained the smallest prediction errors across eight cancer
241 types (Fig. 4a). Moreover, most signatures found by SUITOR were highly similar to the COSMIC
242 signatures (with cosine similarity > 0.8, Fig. 4b) and frequently detected by the other methods
243 (Fig. 4c). In contrast, signatureAnalyzer identified more *de novo* signatures, some of which were
244 not matched to any COSMIC signatures (Fig. 4b).
245

246 Next, we extracted *de novo* signatures combining WGS data from 2,540 tumors (pan-cancer
247 analysis). SUITOR found 22 signatures, eighteen of which could be matched to the COSMIC
248 signatures (Fig. 4b). These signatures had the smallest prediction error (Fig. 4a), compared to
249 signatures detected by the other methods: SUITOR 36,017; sigProfiler 255,111 (>7 times
250 SUITOR's prediction error); signatureAnalyzer 402,409 (>11 times SUITOR's prediction error);
251 and signeR 193,191 (>5 times SUITOR's prediction error). As expected, the signatures
252 commonly found in multiple cancer types (e.g., SBS1, SBS2 and SBS13) could be identified when
253 combining all cancer types together, while signatures specific to a single cancer type (e.g.,
254 SBS24 specific to liver cancer) were absent in the combined signature analysis (Fig. 4c). When
255 we clustered 2,540 tumors based on signature contributions estimated by SUITOR, four clusters
256 emerged in the t-SNE plot (Fig. 5a). Liver tumors formed a distinct cluster, possibly due to its
257 specific signature SBS24 caused by aflatoxin exposure; the remaining clusters included: i) a
258 subset of lymphomas; ii) the majority of kidney tumors; iii) all remaining tumors. Although the
259 liver tumors were separated from the other tumors in the t-SNE plots also by the other
260 methods (Fig. 5b-d), the separation of lymphomas and kidney tumors was less clear. For
261 example, kidney tumors and lymphoma were mixed with other cancer types in the t-SNE plot
262 from signatureAnalyzer.
263

264 **External validation of breast cancer mutational signatures**

265 We validated the nine PCAWG breast cancer signatures (based on 194 breast tumors) using an
266 independent WGS set of 440 breast tumors of the Sanger breast cancer (BRCA) study from the
267 same ethnicity[37]. SUITOR (Fig. 6a and Supplementary Table 5) and signeR (Supplementary Table

268 6) identified nine breast cancer signatures in PCAWG and validated eight in the Sanger BRCA
269 study (with cosine similarity > 0.8); sigProfiler identified eight signatures and confirmed seven
270 (Supplementary Table 7); signatureAnalyzer identified twelve and validated eight
271 (Supplementary Table 8). Overall, six signatures (SBS1,2,8,13,17b and 18) were identified in
272 both studies by all methods, while the flat featureless signature SBS5 could not be validated by
273 any method.
274
275 Besides validating eight PCAWG breast cancer signatures, SUITOR found four additional
276 signatures in the Sanger BRCA study (Fig. 6a and Supplementary Table 9). Two of them were
277 highly similar to COSMIC signatures SBS26 and SBS30 (cosine similarity > 0.93) and were
278 identified by the other three methods as well; the other two (similar to SBS3 and SBS6) were
279 also detected by signatureAnalyzer and/or signeR. Similarly, three other methods found few
280 more signatures as well (Supplementary Tables 10-12). These findings suggest that there likely
281 exist additional signatures in the Sanger BRCA study that are missed in the PCAWG breast
282 cancer study because of either the larger sample size or specific operative mutational processes
283 (e.g., BRCA1 mutation carriers with signature SBS3) in Sanger BRCA study.
284
285 Finally, as an example of clinical utility of the signatures estimated by SUITOR, we stratified the
286 440 breast tumors of the Sanger BRCA study using the signature contributions. Four signature
287 clusters were found; two dominant clusters (G3 and G4) included overall 430 tumors (Fig. 6b).
288 Compared to the G4 subgroup, the G3 subgroup showed significantly higher contributions of
289 the nine signatures (Supplementary Fig. 8; Supplementary Table 13) and significantly lower

290 contributions of the de novo signature A (similar to COSMIC signature SBS1 associated with
291 aging). We found a number of clinical factors associated with the subgroups G3 and G4,
292 including age at diagnosis and tumor grade (Supplementary Table 14). The singular most
293 important associated factor was the molecular subtype: triple negative breast cancers were
294 significantly enriched in the subgroup G3 (Fig. 6c; odds ratio = 25.1, P-value < 2.2×10^{-16}, two-
295 sided Fisher's exact test).
296
297 **Discussion**
298 It's crucial to select the correct number of *de novo* mutational signatures for a cancer genomics
299 study. Here we present SUITOR that selects the number of signatures through cross-validation
300 to minimize the prediction error in the validation set. We have shown how SUITOR outperforms
301 common existing methods most of the time. *In vitro* studies show that SUITOR is capable of
302 retrieving the correct number and profiles of both endogenous and exogenous signatures,
303 allowing the correct stratification of tumor subclones exposed to distinct mutagens. *In silico*
304 simulation studies show that SUITOR can detect common signatures in all replicates and rare
305 signatures (as low as 1%) in the majority of replicates. Applications to *in vivo* eight PCAWG
306 cancer types show that SUITOR discovers signatures which achieve the lowest prediction errors
307 in the testing sets. Most of these signatures are confirmed by other methods and matched to
308 the COSMIC signatures. All except one signature found in PCAWG BRCA study were validated in
309 the independent Sanger BRCA study. The contributions of signatures selected by SUITOR in the
310 Sanger BRCA study are dominated by two clusters, driven by the molecular/histological
311 subtypes.

312 Besides selecting the number of signatures of single base substitution, SUITOR could be used to
313 select the number of signatures of other genomic alterations in tumors, including double base
314 substitutions, small insertion and deletions (indels), and structure variations. In this paper, we
315 used 10-fold cross validation, which is recommended as a good compromise for the bias-
316 variance trade-off regarding the choice of k in k-fold cross validation[38,39]. In addition, we have
317 tried 20-fold cross validation (i.e., 5% of data as validation data) for PCAWG studies, which led
318 to the same number of signatures (results not shown).
319
320 In summary, SUITOR has shown to perform better than other commonly used methods in
321 revealing mutational signatures, the "footprints" engraved in the cancer genomes by operative
322 mutational processes with potentially important etiological or therapeutic implications.
323
324
325 **Methods**

326 **Unsupervised cross-validation for mutational signature analysis**

327 SUITOR aims to select the optimal number of signatures which minimizes the prediction error in
328 the validation set through cross-validation. Here, we describe the steps to create the validation set
329 and the related challenges.
330
331 For a K-fold cross-validation, we divide the catalog matrix **V** into K parts where the Poisson
332 NMF model is fitted on $K-1$ parts as the training set, and the fitted model is validated on the
333 remaining one part as the validation set. The cross-validation is carried out K times with each
334 part served as a validation set once, using the balanced separation[40,41] detailed as follows. In the

335 k^{th} fold ($1 \leq k \leq K$) of a balanced separation, a set of mutation counts

336 $\{v_{np} | p = (n \, mod \, 10) + (k-1) + aK, a = 1, 2, ...\}$ are held out for the nth tumor as validation

337 data, where a is restricted such that $1 \leq p \leq 96$. For example, $(1, 11, \cdots, 91)^{st}$ mutation catalogs

338 of the first tumor are held out in the 1st fold, $(2, 12, \cdots, 92)^{nd}$ mutation catalogs in the 2nd fold

339 and so on. Note that the balanced separation keeps equal number of retained mutation catalogs

340 for each tumor in the training set, which is computationally more stable than randomly splitting

341 $\mathbf{V}$ into the training and validation sets. The latter may randomly remove a large number of

342 mutation catalogs for a tumor.

343

344 As validation data are hold out, missing data emerge in the training set, the reason for which

345 existing methods of NMF fail. To address this challenge, we extended the Poisson NMF model

346 and propose an expectation/conditional maximization (ECM) algorithm to incorporate the

347 missing data.

348

349 **Expectation/conditional maximization (ECM) algorithm of SUITOR**

350 Let $\mathcal{S}$ be the set of indices of mutation catalog matrix $\mathbf{V}$ such that $\mathcal{S} =$

351 $\{(n,p) | 1 \leq n \leq \mathrm{N} \text{ and } 1 \leq p \leq 96\}$. For a K-fold cross-validation, $\mathcal{S}$ would be divided into K

352 disjoint sets $\mathcal{S}_1, \cdots, \mathcal{S}_K$. For the kth fold, $\mathbf{V}_k^L = \{v_{np} | (n,p) \in \mathcal{S}_k\}$ denotes the validation set and $\mathbf{V}_k^T$

353 $= \{v_{np} | (n,p) \in \mathcal{S} \backslash \mathcal{S}_k\}$ the training set, where $\mathcal{S} \backslash \mathcal{S}_k$ represents the indices of $\mathbf{V}$ excluding ones in

354 $\mathcal{S}_k$. Mutation counts in $\mathcal{S}_k$ will be removed from $\mathbf{V}$ and denote as missing data $\mathbf{M}_k =$

355 $\{m_{np} | (n,p) \in \mathcal{S}_k\}$. The v_{np} in $\mathbf{V}_k^T$ and m_{np} in $\mathbf{M}_k$ are assumed to be independently distributed as a

356 Poisson distribution with the mean $\sum_{j=1}^{r} w_{nj} h_{jp}$. By the scheme of balanced separation, $\mathbf{V}_k^L$ is

357 missing completely at random (MCAR), since $\mathbf{V}_k^L$ is removed from $\mathbf{V}$, independent of values of

$\mathbf{V}_k^T$ and $\mathbf{V}_k^L$. MCAR enables us to propose an ECM algorithm to incorporate missing data and obtain unbiased estimates of $\mathbf{W}$ and $\mathbf{H}$ (ref[36]).

Next, we outline the ECM algorithm in the following iterative steps (details in Supplementary Note 3).

1. Initial step: choose initial values of $\mathbf{M}_k$ and set initial parameters $\mathbf{W^0}$ and $\mathbf{H^0}$.
2. E-step: given the observed data $\mathbf{V}_k^T$ and the parameters $\mathbf{W^t}$ and $\mathbf{H^t}$ of the previous step t, the ECM algorithm calculates the conditional expectation of complete likelihood

$$Q(\mathbf{W},\mathbf{H} \mid \mathbf{W^t},\mathbf{H^t}) = E[\log\{\Pr(\mathbf{V}_k^T,\mathbf{M}_k \mid \mathbf{WH})\} \mid \mathbf{W^t},\mathbf{H^t}\}] = -D_{KL}(\mathbf{V}^* \mid \mathbf{WH}) + C^*,$$

   where C^* is a constant independent of $\mathbf{W}$ and $\mathbf{H}$, v_{np}^* the elements of $\mathbf{V}^*$ as $v_{np}^* = v_{np}$ for $(n,p) \in \mathcal{S} \backslash \mathcal{S}_k$ and $v_{np}^* = E[m_{np}] = \sum_{j=1}^{r} w_{nj}^t h_{jp}^t$ for $(n,p) \in \mathcal{S}_k$.
3. CM1-step: update parameters $\mathbf{W^{t+1}}$ by maximizing $Q(\mathbf{W},\mathbf{H^t} \mid \mathbf{W^t},\mathbf{H^t})$ with respect to $\mathbf{W}$.
4. CM2-step: update parameters $\mathbf{H^{t+1}}$ by maximizing $Q(\mathbf{W^{t+1}},\mathbf{H} \mid \mathbf{W^t},\mathbf{H^t})$ with respect to $\mathbf{H}$.
5. Iterate steps 2 to 4 until convergence.

In the initial step, we use the median of mutation counts in $\mathbf{V}_k^T$ per each mutation catalog as initial values for $\mathbf{M}_k$; other more complicated methods of specifying initial values, such as nearest neighbors, lead to similar results (results not shown). We are aware that the ECM algorithm possibly converges to a local saddle point. To overcome it, we try 300 random initial values $\mathbf{W^0}$ and $\mathbf{H^0}$, which leads to 300 pairs of $\hat{\boldsymbol{W}}_i$ and $\hat{\boldsymbol{H}}_i$, the estimates of $\mathbf{W}$ and $\mathbf{H}$ for the ith initial value,

380 $i = 1, 2, \ldots, 300$. The final reported $\hat{\mathbf{W}}$ and $\hat{\mathbf{H}}$ are the $\hat{\boldsymbol{W}}_i$ and $\hat{\boldsymbol{H}}_i$ which maximize the

381 $\log\left\{\Pr\left(\mathbf{V}_k^T \middle| \hat{\boldsymbol{W}}_l, \hat{\boldsymbol{H}}_l\right)\right\}$ among all $\hat{\boldsymbol{W}}_i's$ and $\hat{\boldsymbol{H}}_i's$.

382

383 **Selecting number of signatures by SUITOR**

384 For a given number of signatures r, we first evaluate the prediction error, i.e., the disparity

385 between the observed validation data $\mathbf{V}_k^L$ and the predicted ones $\hat{\boldsymbol{M}}_k = \mathbf{E}[\mathbf{M}_k] =$

386 $\left\{(\hat{\mathbf{W}}\hat{\mathbf{H}})_{np} \middle| (n,p) \in \mathcal{S}_k\right\}$, for the kth fold, $k = 1,2,\ldots,K$,

387 $$ERR_{r,k} \equiv -\log\left\{\Pr\left(\mathbf{V}_k^L \middle| \hat{\boldsymbol{M}}_k\right)\right\} = D_{KL}\left(\mathbf{V}_k^L \middle| \hat{\boldsymbol{M}}_k\right) - C^*.$$

388 We then evaluate overall prediction error, $ERR_r = \sum_{k=1}^{K} ERR_{r,k}$, across K folds. Since the term

389 C^* is unrelated to $\hat{\mathbf{W}}$ and $\hat{\mathbf{H}}$, it is dropped. Finally, we select the number of signatures r^* which

390 minimizes ERR_r over a range of numbers of signatures $1 \leq r \leq R$.

391

392 **Extracting signature profiles and estimating contributions of signatures**

393 Once the optimal number of signatures r^* is determined by SUITOR, we extract mutational

394 signature profiles $\mathbf{W}$ and estimating contributions $\mathbf{H}$, via maximizing $\log\{\Pr(\mathbf{V} \mid \mathbf{WH})\}$ with the

395 fixed rank r^*. Similar to the ECM algorithm in SUITOR, we evaluate multiple initial values and

396 use $\hat{\mathbf{W}}$ and $\hat{\mathbf{H}}$ which maximizes $\log\left\{\Pr\left(\mathbf{V} \middle| \hat{\mathbf{W}}\hat{\mathbf{H}}\right)\right\}$ to relieve local optima problem.

397 ***In vitro* studies**

398 The datasets of two *in vitro* studies were downloaded from

399 http://medgen.medschl.cam.ac.uk/serena-nik-zainal/. The details of study design and

400 implementation were described previously[2,5]. In these *in vitro* studies, the endogenous and

401 exogenous mutational signatures were experimentally generated *in vitro* and hence the true
402 number of signatures and profiles are known.
403
404 We created the mutation catalog matrix for both studies and applied SUITOR, sigProfiler,
405 signatureAnalyzer and signeR. We chose sigProfiler and signatureAnalyzer, since they have
406 been applied to a number of studies[7,8,18,42-44], and signeR[17] because it utilizes Bayesian
407 information criterion (BIC), a popular model selection criterion for supervised learning. For
408 SUITOR, we used 10-fold cross-validation with 90% of counts in mutation catalog matrix as the
409 training set and the remaining 10% as the validation set. In contrast, the whole mutation catalog
410 matrix **V** was analyzed by sigProfiler, signatureAnalyzer and signeR, respectively under the
411 default setting.
412
413 The first study induced endogenous mutational signatures by CRISPR-Cas9-mediated knockouts
414 of DNA repair genes in an isogenic human cell line. First, we focused on the *MSH6* knockout-
415 induced single base substitution signature, which is characterized by C>T and T>C single base
416 substitutions (~148 substitutions per cell division). We evaluated whether the four methods were
417 able to retrieve the background signature and the *MSH6* knockout-induced signatures. Next, we
418 analyzed the gene-knockout studies with no induced signatures (for genes
419 *CHK2, NEIL1, NUDT1, POLB, POLE* and *POLM*), to evaluate whether the four methods would
420 find false positive signatures in addition to the background signature.
421
422 In the second study, exogenous mutational signatures were created by environmental or
423 therapeutic mutagens. We selected 324 subclones (including 35 control subclones) of human-

424 induced pluripotent stem cell (iPSC) lines, for which the mutations were measured by whole-
425 genome sequencing (WGS). While controls are not exposed to mutagens, each subclone is
426 exposed to one of 79 mutagens, including simulated solar radiation (SSR), dibenzo[a,l]pyrene
427 (DBP) and alkylating agent therapy temozolomide (TMZ). SSR recapitulates the UV-associated
428 signatures and DBP is a potent carcinogen of the polycyclic aromatic hydrocarbons (PAHs)
429 produced when coal, crude oil, or gasoline is burned. For each method, we checked if the correct
430 number of signatures were attained with its impacts on the downstream analyses. Specifically,
431 we investigated whether the retrieved *de novo* signature profiles were highly similar to the true
432 signature profiles. We further explored if signature contributes could separate subclones exposed
433 to the distinctive mutagens, visualized by t-distributed stochastic neighbor embedding (t-SNE[45]).
434

435 ***In silico* simulation design with random mutations**

436 We simulated mutation catalog matrix for 300 tumors directly from the Poisson distribution with
437 the mean lambda, which in turn was drawn from a uniform distribution and varied from 20 to
438 160. We repeated this simulation 20 times and analyzed the simulated catalog matrices by
439 SUITOR, sigProfiler, signatureAnalyzer and signeR.
440

441 ***In silico* simulation design with one signature**

442 We simulated a mutation catalog matrix for 500 tumors and analyzed it by the four methods,
443 each repeated 20 times. We used the signature profile of SBS8 as the true signature profile for **H**
444 and generated the contribution vector **W** from a uniform distribution within the range [20000,
445 40000]. Then the mutation catalog **V** was generated by a Poisson distribution with mean **WH**.
446

447 ***In silico* simulation design with nine signatures**

448 We simulated signatures mimic to the ones observed in the Pan-Cancer Analysis of Whole
449 Genomes (PCAWG) breast cancer study[1]. The nine signatures identified by SUITOR show
450 various signature contributions and signature profiles; some signatures contribute to all tumors
451 (e.g., SBS1 and SBS5, present in 100% of tumors; Supplementary Table 4) while others
452 contribute to a few tumors (e.g., SBS41, present in 6% of tumors) and even to one (SBS40) or
453 two tumors (SBS8); some signature profiles are spiky (e.g., SBS1 and SBS2/13; Supplementary
454 Fig. 5) while others are relatively flat (e.g., SBS5).

455

456 Specifically, we generated mutation catalog matrices similar to $\mathbf{V}^{\mathrm{BR}}$, the mutation catalog matrix
457 of PCAWG breast cancer study. $\mathbf{V}^{\mathrm{BR}}$ is approximated by $\mathbf{W}^{\mathrm{BR}}\mathbf{H}$, for which $\mathbf{H}$ contains the
458 COSMIC signature profiles and $\mathbf{W}^{\mathrm{BR}}$ is the corresponding signature contribution matrix
459 (downloaded from https://www.synapse.org/#!Synapse:syn11738669). We removed signatures
460 with zero contributions to all tumors and chose 9 signatures to compose the signature profile
461 matrix $\mathbf{H}$ of size 9×96. With $\mathbf{H}$ fixed, we took bootstrap samples $\mathbf{W}_{\boldsymbol{boot}}^{\boldsymbol{BR}}$ from each column of
462 matrix $\mathbf{W}^{\mathrm{BR}}$, and generated $\mathbf{V}_{\boldsymbol{boot}}^{\boldsymbol{BR}}$ which follows a Poisson distribution with mean $\mathbf{W}_{\boldsymbol{boot}}^{\boldsymbol{BR}}\,\mathbf{H}$. Due
463 to the dependencies between SBS1 and SBS5 as well as between SBS2 and SBS13, their
464 contributions are resampled jointly while the contributions of other signatures are sampled
465 individually. We simulated 20 mutation catalog matrices for 200 tumors, and each was analyzed
466 by four methods respectively.

467

468 ***In vivo* human cancer genomics studies**

469 We analyzed 2, 540 tumors across 22 cancer types of PCAWG[1], including 321 tumors of
470 hepatocellular carcinoma, 286 tumors of prostate adenocarcinoma, 237 tumors of
471 pancreatic adenocarcinoma, 194 tumors of breast adenocarcinoma, 146 tumors of central nervous
472 system medulloblastoma, 143 tumors of renal cell carcinoma,112 tumors of ovary
473 adenocarcinoma and 100 cases of B-cell non-Hodgkin lymphoma. Other cancer types have less
474 than 100 tumors per cancer type. The tumors were whole genome sequenced and datasets of the
475 somatic mutation calls were downloaded from
476 https://www.synapse.org/#!Synapse:syn11726620. The hypermutator tumors with mutation
477 burden more than 10 mutations/Mb were excluded[46]. For each cancer type, we applied SUITOR,
478 sigProfiler, signatureAnalyzer and signeR to select the number of signatures and estimate
479 signature contributions and profiles.
480
481 To compare the prediction errors, we split the mutation catalog matrix into a training set (90% of
482 counts in the mutation catalog matrix), a validation set (5%) and a testing set (5%). For SUITOR,
483 the training set was used to fit the probabilistic NMF model with multiple numbers of signatures
484 and the validation set to select the number of signatures. The other methods used both the
485 training and validation sets to select the number of signatures. Next, we compared the prediction
486 errors of selected signatures by each method on the testing set. For sigProfiler, signatureAnalyzer
487 and signeR, we imputed missing training data by medians of available mutation counts per each
488 mutational catalog, applied each method, predicted the testing data and calculated the prediction
489 error as SUITOR did. For SUITOR, it could handle missing data and predict the testing data by
490 the ECM algorithm.
491

492 **Sanger whole genome sequencing breast cancer study**

493 The Sanger whole genome breast cancer (BRCA) study sequenced 560 breast tumors. The
494 somatic mutation calls files were downloaded from https://medgen.medschl.cam.ac.uk/serena-
495 nik-zainal/. Among 560 breast tumors, 110 tumors were included in PCAWG and hence
496 excluded from this validation study. Ten hypermutator tumors were also excluded. We applied
497 SUITOR, sigProfiler, signatureAnalyzer and signeR to a) select the number of signatures and
498 estimate signature contributions and profiles; b) compare the signatures with ones detected in the
499 PCAWG breast cancer study; and c) investigate if additional signatures are found in Sanger
500 whole genome breast cancer study. In addition, we stratified the tumors based on mutation
501 contributions and associated the signature clusters with epidemiological or clinical
502 characteristics.

503

504 **Software webpages:**

505

506 SUITOR: https://github.com/binzhulab/SUITOR

507

508 sigProfiler: v1.0.6 is installed and used by following instructions in
509 https://github.com/AlexandrovLab/SigProfilerExtractor.

510

511 signatureAnalyzer: version information is not available but is installed by following instructions
512 in https://github.com/broadinstitute/getzlab-SignatureAnalyzer.

513

514 signeR: v1.12.0 is downloaded from

515 https://bioconductor.org/packages/release/bioc/html/signeR.html.

516

517 sigProfiler and signatureAnalyzer are used in python version 3.7.5 while SUITOR and signeR

518 are used in R version 3.6.3. Signature profiles plot is drawn based on R package

519 MutationalPatterns from

520 https://bioconductor.org/packages/release/bioc/html/MutationalPatterns.html with slight

521 modification to add graphical parameters.

522 **Acknowledgment**

523 This research was supported by the Intramural Research Program of the National Institutes of

524 Health, National Cancer Institute, Division of Cancer Epidemiology and Genetics (DCEG). This

525 study utilized the high-performance computational capabilities of the Biowulf Linux cluster at

526 the National Institutes of Health, Bethesda, MD: https://biowulf.nih.gov. We would like to thank

527 Bill Wheeler (Information Management Services) for computation support and Dr. Paul Albert

528 (Biostatistics Branch of DCEG) and Dr. Ludmil Alexandrov (University of California San

529 Diego) for helpful comments. Conflict of Interest: None declared.

530

531 **Reference:**

532

533 1. Alexandrov, L.B. *et al.* The repertoire of mutational signatures in human cancer. *Nature*
534 **578**, 94-101 (2020).
535 2. Kucab, J.E. *et al.* A Compendium of Mutational Signatures of Environmental Agents. *Cell*
536 **177**, 821-836 e16 (2019).
537 3. Alexandrov, L.B. *et al.* Mutational signatures associated with tobacco smoking in human
538 cancer. *Science* **354**, 618-622 (2016).
539 4. Letouze, E. *et al.* Mutational signatures reveal the dynamic interplay of risk factors and
540 cellular processes during liver tumorigenesis. *Nat Commun* **8**, 1315 (2017).

541 5. Zou, X. *et al.* Validating the concept of mutational signatures with isogenic cell models.
542 *Nat Commun* **9**, 1744 (2018).
543 6. Polak, P. *et al.* A mutational signature reveals alterations underlying deficient
544 homologous recombination repair in breast cancer. *Nat Genet* **49**, 1476-1486 (2017).
545 7. Haradhvala, N.J. *et al.* Distinct mutational signatures characterize concurrent loss of
546 polymerase proofreading and mismatch repair. *Nat Commun* **9**, 1746 (2018).
547 8. Petljak, M. *et al.* Characterizing Mutational Signatures in Human Cancer Cell Lines
548 Reveals Episodic APOBEC Mutagenesis. *Cell* **176**, 1282-1294 e20 (2019).
549 9. Drost, J. *et al.* Use of CRISPR-modified human stem cell organoids to study the origin of
550 mutational signatures in cancer. *Science* **358**, 234-238 (2017).
551 10. Secrier, M. *et al.* Mutational signatures in esophageal adenocarcinoma define
552 etiologically distinct subgroups with therapeutic relevance. *Nat Genet* **48**, 1131-41
553 (2016).
554 11. Staaf, J. *et al.* Whole-genome sequencing of triple-negative breast cancers in a
555 population-based clinical study. *Nat Med* **25**, 1526-1533 (2019).
556 12. Connor, A.A. *et al.* Association of Distinct Mutational Signatures With Correlates of
557 Increased Immune Activity in Pancreatic Ductal Adenocarcinoma. *JAMA Oncol* **3**, 774-
558 783 (2017).
559 13. Li, X. *et al.* Distinct Subtypes of Gastric Cancer Defined by Molecular Characterization
560 Include Novel Mutational Signatures with Prognostic Capability. *Cancer Res* **76**, 1724-32
561 (2016).
562 14. Gehring, J.S., Fischer, B., Lawrence, M. & Huber, W. SomaticSignatures: inferring
563 mutational signatures from single-nucleotide variants. *Bioinformatics* **31**, 3673-5 (2015).
564 15. Alexandrov, L.B., Nik-Zainal, S., Wedge, D.C., Campbell, P.J. & Stratton, M.R.
565 Deciphering signatures of mutational processes operative in human cancer. *Cell Rep* **3**,
566 246-59 (2013).
567 16. Fischer, A., Illingworth, C.J., Campbell, P.J. & Mustonen, V. EMu: probabilistic inference
568 of mutational processes and their localization in the cancer genome. *Genome Biol* **14**,
569 R39 (2013).
570 17. Rosales, R.A., Drummond, R.D., Valieris, R., Dias-Neto, E. & da Silva, I.T. signeR: an
571 empirical Bayesian approach to mutational signature discovery. *Bioinformatics* **33**, 8-16
572 (2017).
573 18. Kim, J. *et al.* Somatic ERCC2 mutations are associated with a distinct genomic signature
574 in urothelial tumors. *Nat Genet* **48**, 600-606 (2016).
575 19. Rosenthal, R., McGranahan, N., Herrero, J., Taylor, B.S. & Swanton, C.
576 DeconstructSigs: delineating mutational processes in single tumors distinguishes DNA
577 repair deficiencies and patterns of carcinoma evolution. *Genome Biol* **17**, 31 (2016).
578 20. Huang, X., Wojtowicz, D. & Przytycka, T.M. Detecting presence of mutational signatures
579 in cancer with confidence. *Bioinformatics* **34**, 330-337 (2018).
580 21. Maura, F. *et al.* A practical guide for mutational signature analysis in hematological
581 malignancies. *Nat Commun* **10**, 2969 (2019).
582 22. Degasperi, A. *et al.* A practical framework and online tool for mutational signature
583 analyses show inter-tissue variation and driver dependencies. *Nat Cancer* **1**, 249-263
584 (2020).
585 23. Schwarz, G. Estimating the dimension of a model. *The annals of statistics* **6**, 461-464
586 (1978).
587 24. Tan, V.Y. & Févotte, C. Automatic relevance determination in nonnegative matrix
588 factorization with the β-divergence. *IEEE Trans Pattern Anal Mach Intell* **35**, 1592-605
589 (2013).
590 25. Zhang, Y. & Yang, Y. Cross-validation for selecting a model selection procedure. *Journal
591 of Econometrics* **187**, 95-112 (2015).

26. Arlot, S. & Celisse, A. A survey of cross-validation procedures for model selection. *Statistics surveys* **4**, 40-79 (2010).
27. Dyrskjot, L. *et al.* Identifying distinct classes of bladder carcinoma using microarrays. *Nat Genet* **33**, 90-6 (2003).
28. Byrne, R.P. *et al.* Dutch population structure across space, time and GWAS design. *Nat Commun* **11**, 4556 (2020).
29. Yu, J. *et al.* Lymph node metastasis prediction of papillary thyroid carcinoma based on transfer learning radiomics. *Nat Commun* **11**, 4807 (2020).
30. Meng, X.-L. & Rubin, D.B. Maximum Likelihood Estimation via the ECM Algorithm: A General Framework. *Biometrika* **80**, 267-278 (1993).
31. Févotte, C. & Cemgil, A.T. Nonnegative matrix factorizations as probabilistic inference in composite models. in *2009 17th European Signal Processing Conference* 1913-1917 (2009).
32. Gaussier, E. & Goutte, C. Relation between PLSA and NMF and implications. in *Proceedings of the 28th annual international ACM SIGIR conference on Research and development in information retrieval* 601–602 (Association for Computing Machinery, Salvador, Brazil, 2005).
33. Ding, C., Li, T. & Peng, W. Nonnegative matrix factorization and probabilistic latent semantic indexing: equivalence, chi-square statistic, and a hybrid method. in *Proceedings of the 21st national conference on Artificial intelligence - Volume 1* 342–347 (AAAI Press, Boston, Massachusetts, 2006).
34. Lee, D.D. & Seung, H.S. Learning the parts of objects by non-negative matrix factorization. *Nature* **401**, 788-91 (1999).
35. Friedman, J., Hastie, T. & Tibshirani, R. *The elements of statistical learning*, (Springer series in statistics New York, 2001).
36. Little, R.J. & Rubin, D.B. *Statistical analysis with missing data*, (John Wiley & Sons, 2019).
37. Nik-Zainal, S. *et al.* Landscape of somatic mutations in 560 breast cancer whole-genome sequences. *Nature* **534**, 47-54 (2016).
38. Kohavi, R. A study of cross-validation and bootstrap for accuracy estimation and model selection. in *Proceedings of the 14th international joint conference on Artificial intelligence - Volume 2* 1137–1143 (Morgan Kaufmann Publishers Inc., Montreal, Quebec, Canada, 1995).
39. Breiman, L. & Spector, P. Submodel Selection and Evaluation in Regression. The X-Random Case. *International Statistical Review / Revue Internationale de Statistique* **60**, 291-319 (1992).
40. Bro, R., Kjeldahl, K., Smilde, A.K. & Kiers, H.A.L. Cross-validation of component models: A critical look at current methods. *Analytical and Bioanalytical Chemistry* **390**, 1241-1251 (2008).
41. Wold, S. Cross-Validatory Estimation of the Number of Components in Factor and Principal Components Models. *Technometrics* **20**, 397-405 (1978).
42. Xue, R. *et al.* Genomic and Transcriptomic Profiling of Combined Hepatocellular and Intrahepatic Cholangiocarcinoma Reveals Distinct Molecular Subtypes. *Cancer Cell* **35**, 932-947 e8 (2019).
43. Rose Li, Y. *et al.* Mutational signatures in tumours induced by high and low energy radiation in Trp53 deficient mice. *Nat Commun* **11**, 394 (2020).
44. Kasar, S. *et al.* Whole-genome sequencing reveals activation-induced cytidine deaminase signatures during indolent chronic lymphocytic leukaemia evolution. *Nat Commun* **6**, 8866 (2015).
45. Maaten, L.v.d. & Hinton, G. Visualizing data using t-SNE. *Journal of machine learning research* **9**, 2579-2605 (2008).

46. Campbell, B.B. *et al.* Comprehensive Analysis of Hypermutation in Human Cancer. *Cell* **171**, 1042-1056 e10 (2017).

Figure legends:

Fig.1 A schematic overview of SUITOR. This schematic diagram illustrates how SUITOR selects the number of *de novo* mutational signatures. Details are given in Results. Each row of the mutation catalog matrix $\boldsymbol{V}$ represents a tumor, each column a mutation catalog. The bottom left shows prediction error curves in the training set (blue) and validation set (red), which are manually drawn for the illustration purpose, with the red dot representing the minimal prediction error in the validation set. ECM algorithm: expectation/conditional maximization algorithm; CM-steps: conditional maximization steps; E-step: expectation step; $\mathbf{W}$: signature contribution matrix of size $\mathrm{N} \times r$, N the number of tumor and r the number of signatures; $\mathbf{H}$: signature profile matrix of size $r \times 96$; $Q(\boldsymbol{W},\boldsymbol{H} \mid \boldsymbol{W^t},\boldsymbol{H^t})$: conditional expectation of complete likelihood of $\mathbf{W}$ and $\mathbf{H}$ at the $(t+1)$-th step, given estimated $\boldsymbol{W^t}$ and $\boldsymbol{H^t}$ in the t-th step of ECM algorithm.

Fig.2 *In vitro* evaluation of SUITOR and other methods. a) Prediction errors of SUITOR for the training and validation sets of *in vitro* knockout study of DNA repair gene *MSH6*. The red dot denotes the number of signatures with the minimal prediction error in the validation set. b) Profiles of single base substitution signature estimated by SUITOR in *MSH6* gene knockout study. The x-axis indicates the 5' and 3' nucleotides for each substitution type (e.g., T[C>A]C, cytosine to adenine substitution with 5' thymine and 3' cytosine). The top panel: the true and estimated background signatures (cosine similarity=0.991; cosine similarity=1 suggests two profiles being identical.); the bottom panel: the true and estimated *MSH6* knockout-induced

666 signatures (cosine similarity=0.997). c) Prediction errors by SUITOR for the training and
667 validation sets of *in vitro* study of environmental or therapeutic mutagens. The red dot
668 indicates the minimal prediction error in the validation set achieved by ten signatures, including
669 one background signature and nine mutagen-induced signatures. d) Signatures discovered from
670 the *in vitro* study of environmental or therapeutic mutagens by four methods. Methods which
671 could identify a given mutagen are enclosed in paratheses. ENU: N-ethyl-N-nitrosourea; 6-
672 Nitrochrysene+S9: 6-Nitrochrysene mixed with S9 rodent liver-derived metabolic enzyme; DES:
673 diethyl sulfate; SSR: simulated solar radiation; AAI: aristolochic acid I; 1,2-DMH+S9: 1,2-
674 dimethylhydrazine mixed with S9 rodent liver-derived metabolic enzyme; BPDE:
675 benzo[a]pyrene-7,8-dihydrodiol-9,10-epoxide; DBADE: dibenz[a,h]anthracene diol-epoxide.

676

677 **Fig.3 *In silico* evaluation of SUITOR and other methods.** a) The signature profiles of the true
678 mutational signature and the ones discovered by each method for a replicate. b) The number of
679 replicates in which a given signature will be detected by each method; the rare signatures SBS8
680 and SBS41 were discovered in 12, 6, 14 and 6 replicates, and 17, 7, 19 and 11 replicates over
681 total 20 replicates by SUITOR, sigProfiler, signatureAnalyzer and signeR, respectively.

682

683 **Fig.4 Mutational signature results of eight cancer studies of PCAWG.** a) The prediction errors
684 of SUITOR, sigProfiler, signatureAnalyzer and signeR for eight cancer types (scale on the left-
685 side Y axis) and for 2,540 tumors across 22 cancer types together, namely Pan-Cancer (scale on
686 the right-side Y axis). SD: standard deviation. b) The number of signatures identified by each
687 method. The shaded bars and the numbers above indicate the number of signatures whose

688 profiles could be matched to COSMIC profiles (with cosine similarity > 0.8). c) The cosine
689 similarities between *de novo* signatures and COSMIC signatures. Only the matched pairs are
690 shown (with cosine similarity > 0.8). The higher the cosine similarity the better match to a
691 COSMIC signature profile. The cosine similarity equivalent to one denotes a perfect match.
692
693 **Fig.5 The t-SNE visualization of clustering patterns for 2,540 tumors across 22 cancer types**
694 **based on signature contributions.** Signature contributions are estimated by four methods: (a)
695 SUITOR, (b) sigProfiler, (c) signatureAnalyzer and (d) signeR. Each dot represents a tumor and is
696 colored by the cancer type.
697
698 **Fig.6 The results of Sanger breast cancer study by SUITOR.** a) The heatmap of cosine similarity
699 between *de novo* signatures detected in the PCAWG breast cancer (BRCA) study and *de novo*
700 signatures in the Sanger BRCA study. The signatures of the Sanger BRCA study are annotated by
701 COSMIC signatures (if cosine similarities > 0.8) among parentheses. For example, DNSigA (SBS1)
702 refers to *de novo* signature A (DNSigA) being annotated by COSMIC signature SBS1. b) The
703 heatmap of signature contributions estimated by SUITOR with hierarchical clustering in the
704 Sanger BRCA study. The number of tumors included in each signature cluster is shown among
705 parentheses on the top of the heatmap. Q1, Q2, Q3: the 1st, 2nd and 3rd quantiles of signature
706 contributions. c) The t-SNE visualization of tumors in G3 and G4 signature clusters, color-coded
707 by signature clusters and molecular subtypes. TNBC: triple negative breast cancer.

Figure 1

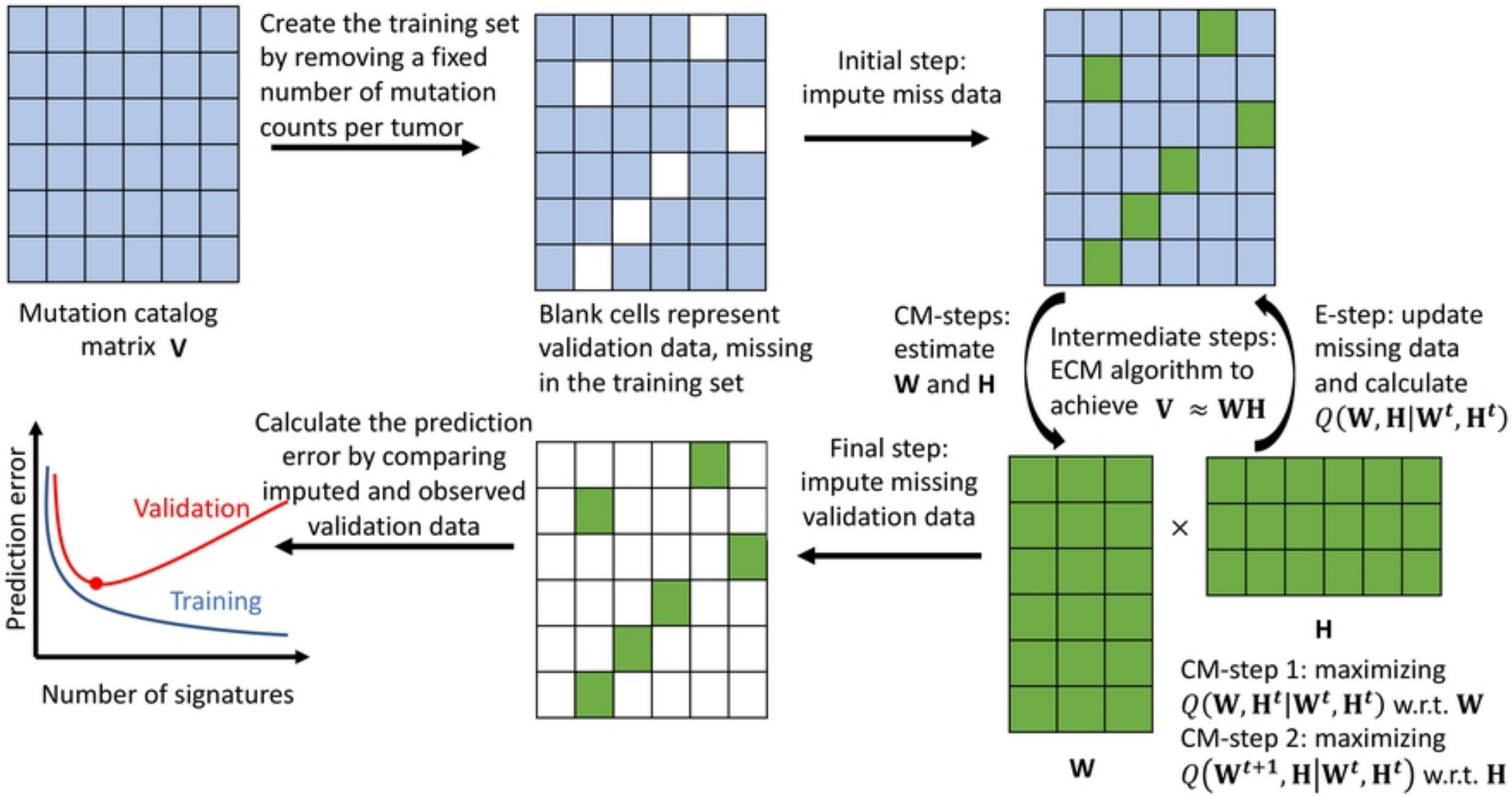
Mutation catalog matrix **V**
Create the training set by removing a fixed number of mutation counts per tumor
Blank cells represent validation data, missing in the training set
Initial step: impute miss data
CM-steps: estimate **W** and **H**
Intermediate steps: ECM algorithm to achieve $\mathbf{V} \approx \mathbf{WH}$
E-step: update missing data and calculate $Q(\mathbf{W},\mathbf{H}|\mathbf{W}^t,\mathbf{H}^t)$
W
×
H
CM-step 1: maximizing $Q(\mathbf{W},\mathbf{H}^t|\mathbf{W}^t,\mathbf{H}^t)$ w.r.t. **W**
CM-step 2: maximizing $Q(\mathbf{W}^{t+1},\mathbf{H}|\mathbf{W}^t,\mathbf{H}^t)$ w.r.t. **H**
Final step: impute missing validation data
Calculate the prediction error by comparing imputed and observed validation data
Prediction error
Validation
Training
Number of signatures

Figure 2

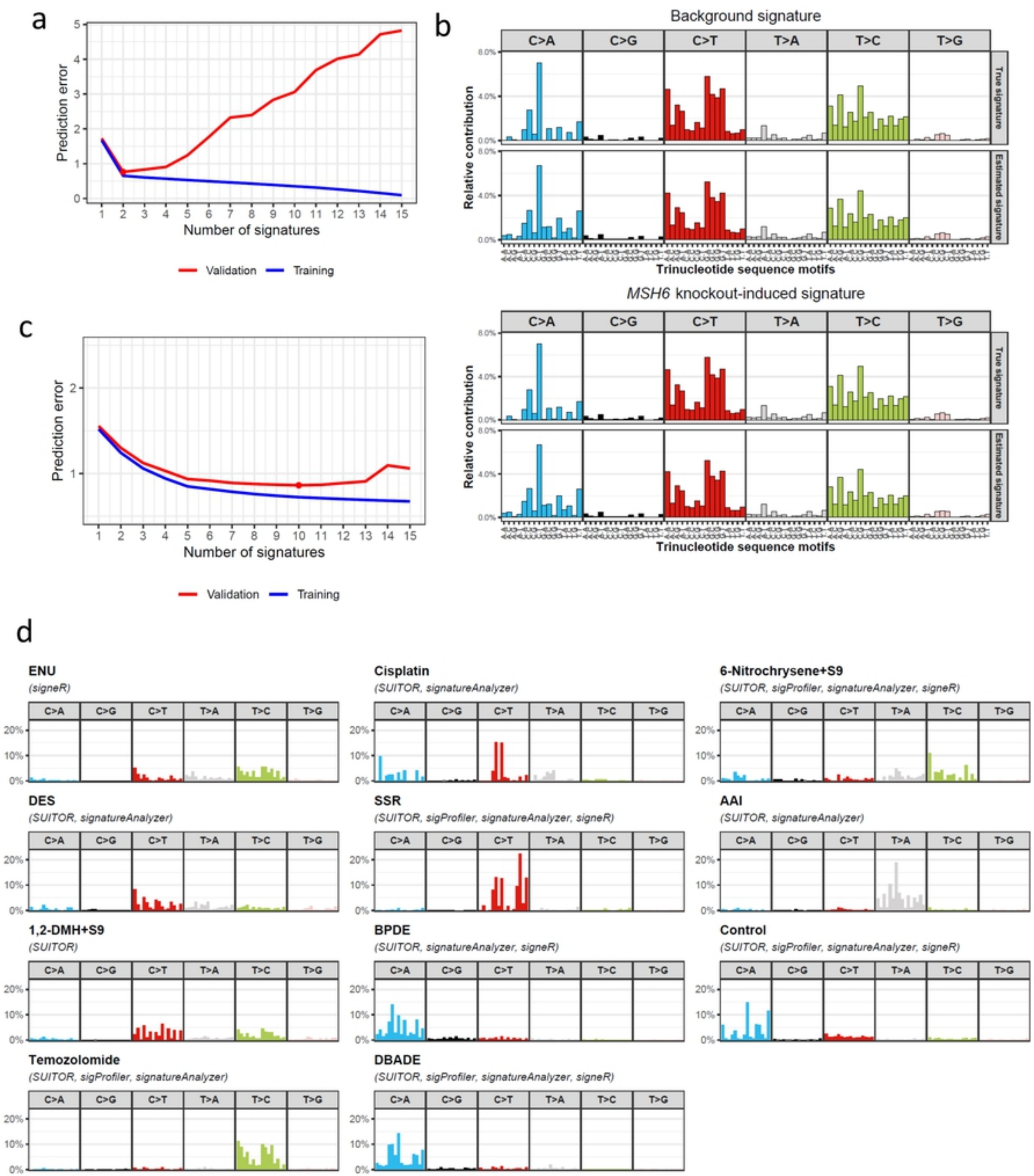
a
Prediction error
Number of signatures
Validation
Training
b
Background signature
C>A
C>G
C>T
T>A
T>C
T>G
Relative contribution
True signature
Estimated signature
Trinucleotide sequence motifs
MSH6 knockout-induced signature
c
Prediction error
Number of signatures
Validation
Training
d
ENU
(signeR)
Cisplatin
(SUITOR, signatureAnalyzer)
6-Nitrochrysene+S9
(SUITOR, sigProfiler, signatureAnalyzer, signeR)
DES
(SUITOR, signatureAnalyzer)
SSR
(SUITOR, sigProfiler, signatureAnalyzer, signeR)
AAI
(SUITOR, signatureAnalyzer)
1,2-DMH+S9
(SUITOR)
BPDE
(SUITOR, signatureAnalyzer, signeR)
Control
(SUITOR, sigProfiler, signatureAnalyzer, signeR)
Temozolomide
(SUITOR, sigProfiler, signatureAnalyzer)
DBADE
(SUITOR, sigProfiler, signatureAnalyzer, signeR)

Figure 3

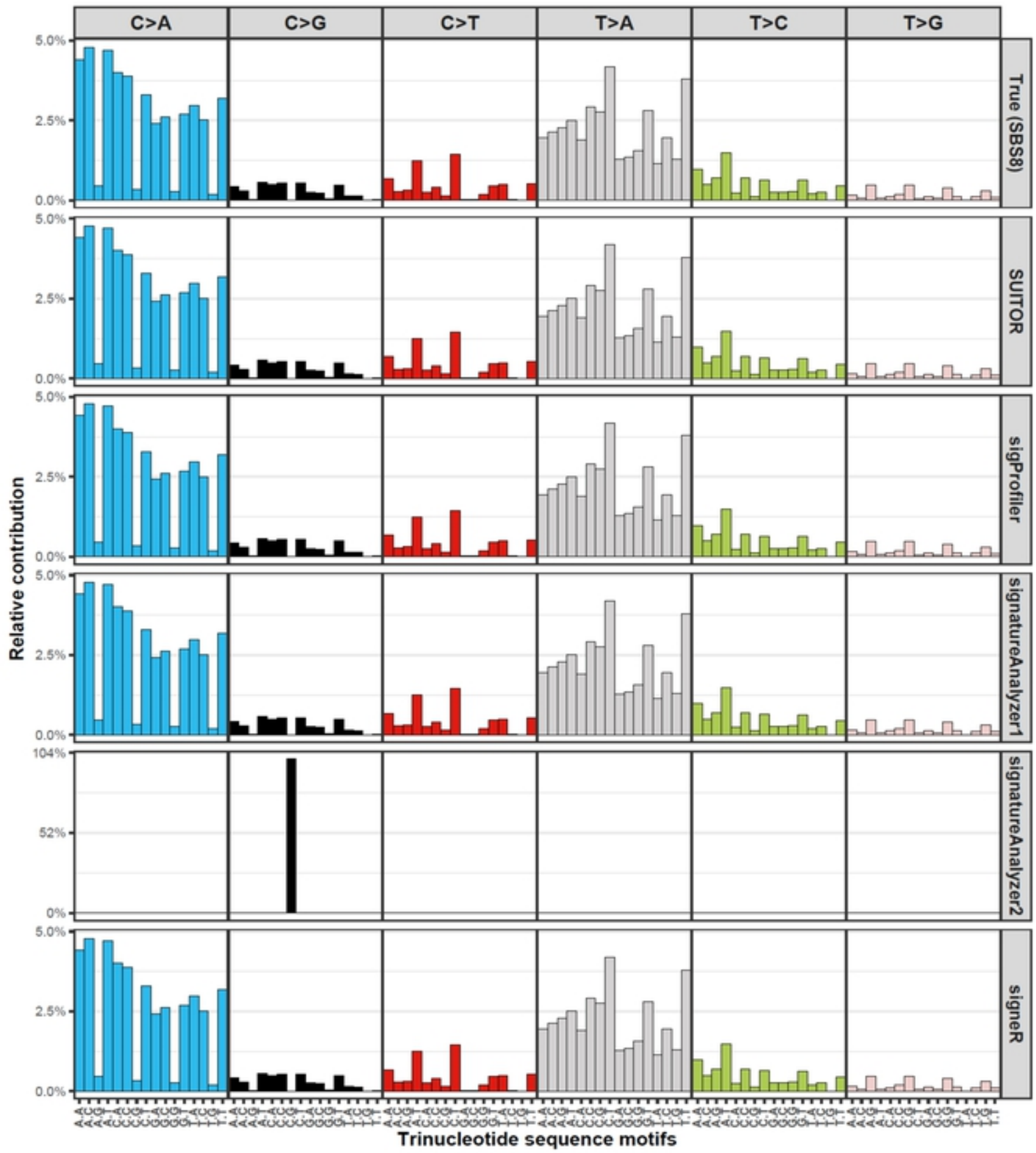
a
C>A
C>G
C>T
T>A
T>C
T>G
True (SBS8)
SUITOR
sigProfiler
signatureAnalyzer1
signatureAnalyzer2
signeR
Relative contribution
5.0%
2.5%
0.0%
104%
52%
0%
Trinucleotide sequence motifs

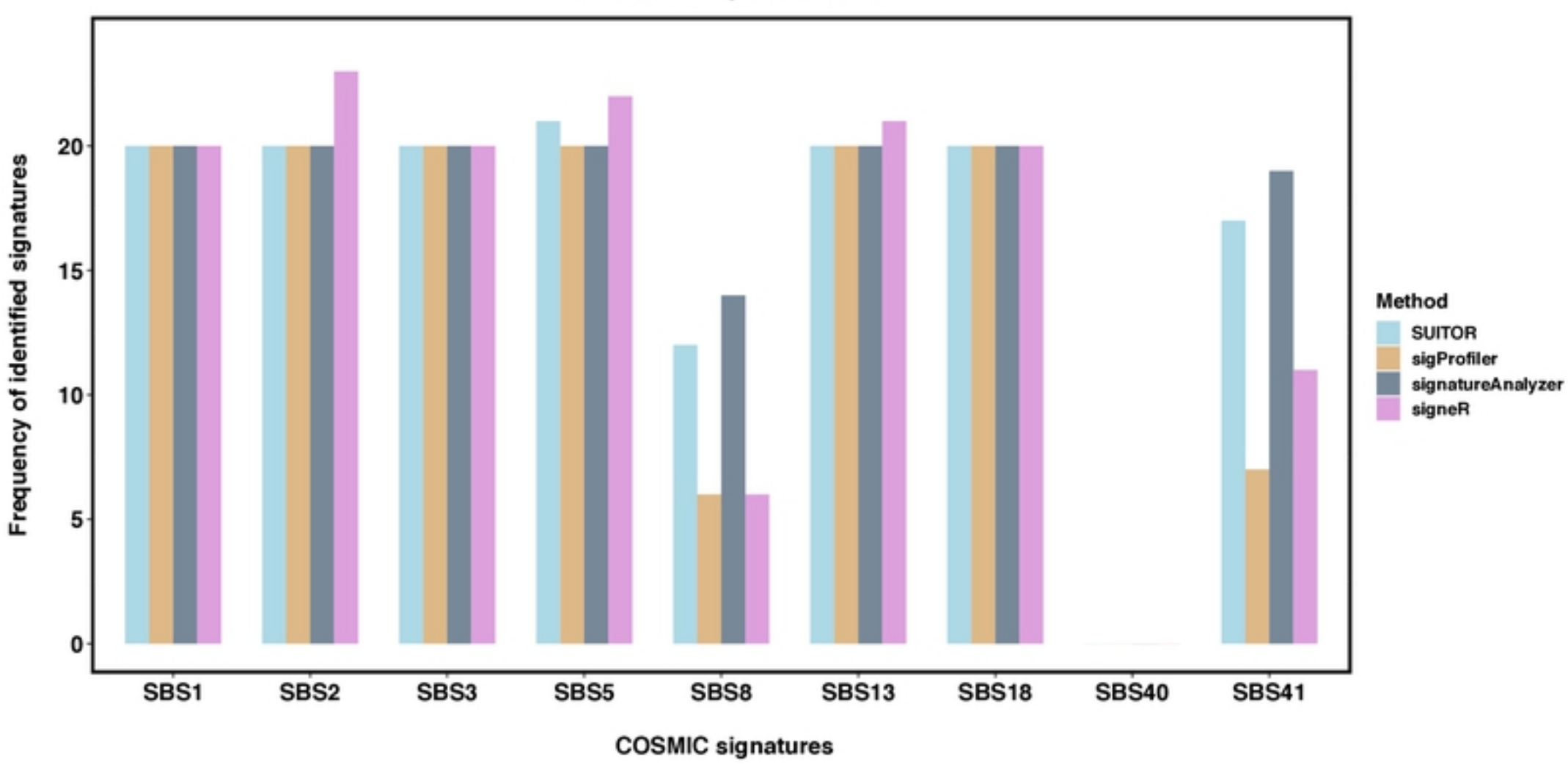
b
Frequency of identified signatures
0
5
10
15
20
SBS1
SBS2
SBS3
SBS5
SBS8
SBS13
SBS18
SBS40
SBS41
COSMIC signatures
Method
SUITOR
sigProfiler
signatureAnalyzer
signeR

Figure 4

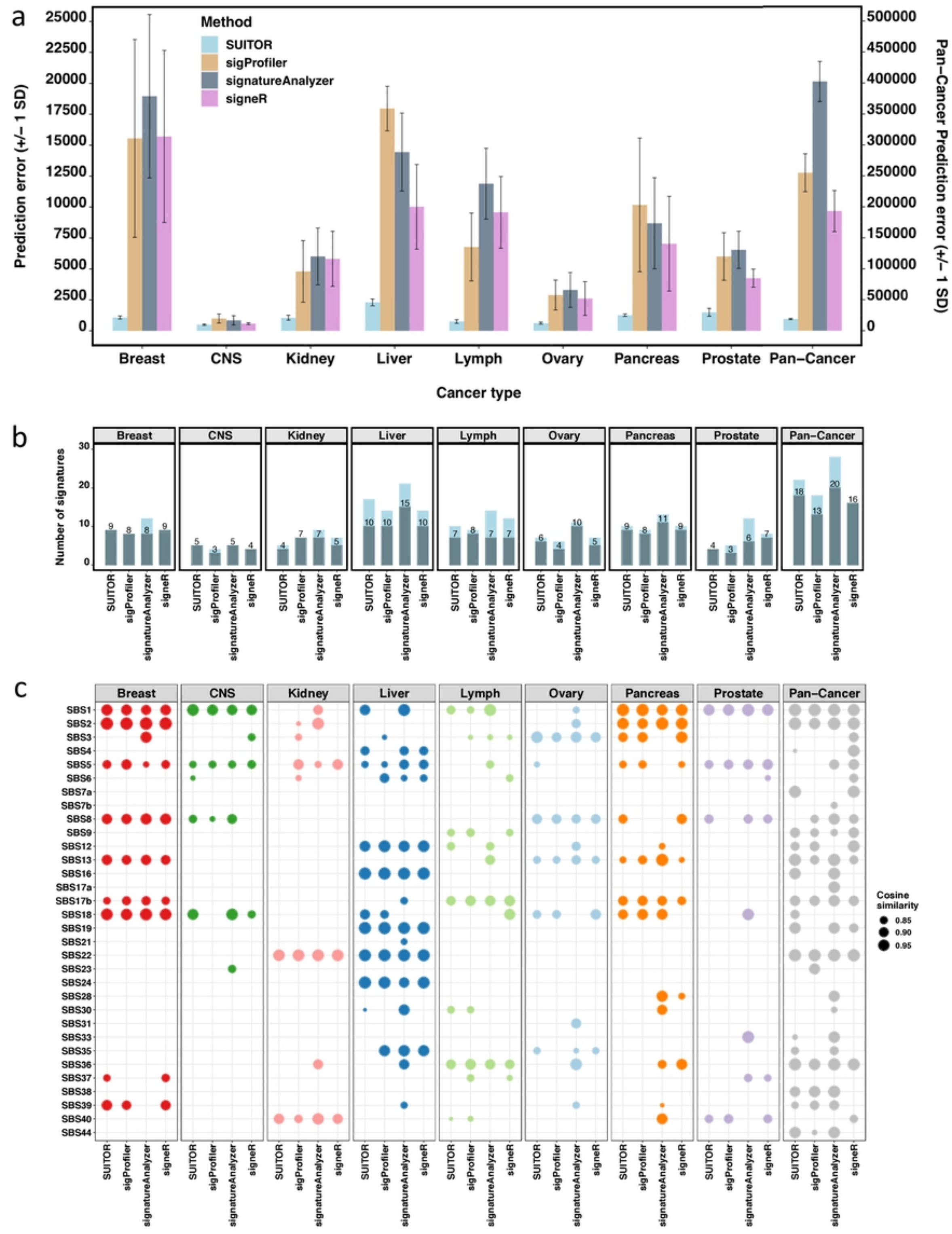
a
Method
SUITOR
sigProfiler
signatureAnalyzer
signeR
Prediction error (+/– 1 SD)
Pan–Cancer Prediction error (+/– 1 SD)
Breast
CNS
Kidney
Liver
Lymph
Ovary
Pancreas
Prostate
Pan–Cancer
Cancer type
b
Number of signatures
c
Cosine similarity
0.85
0.90
0.95

Figure 5

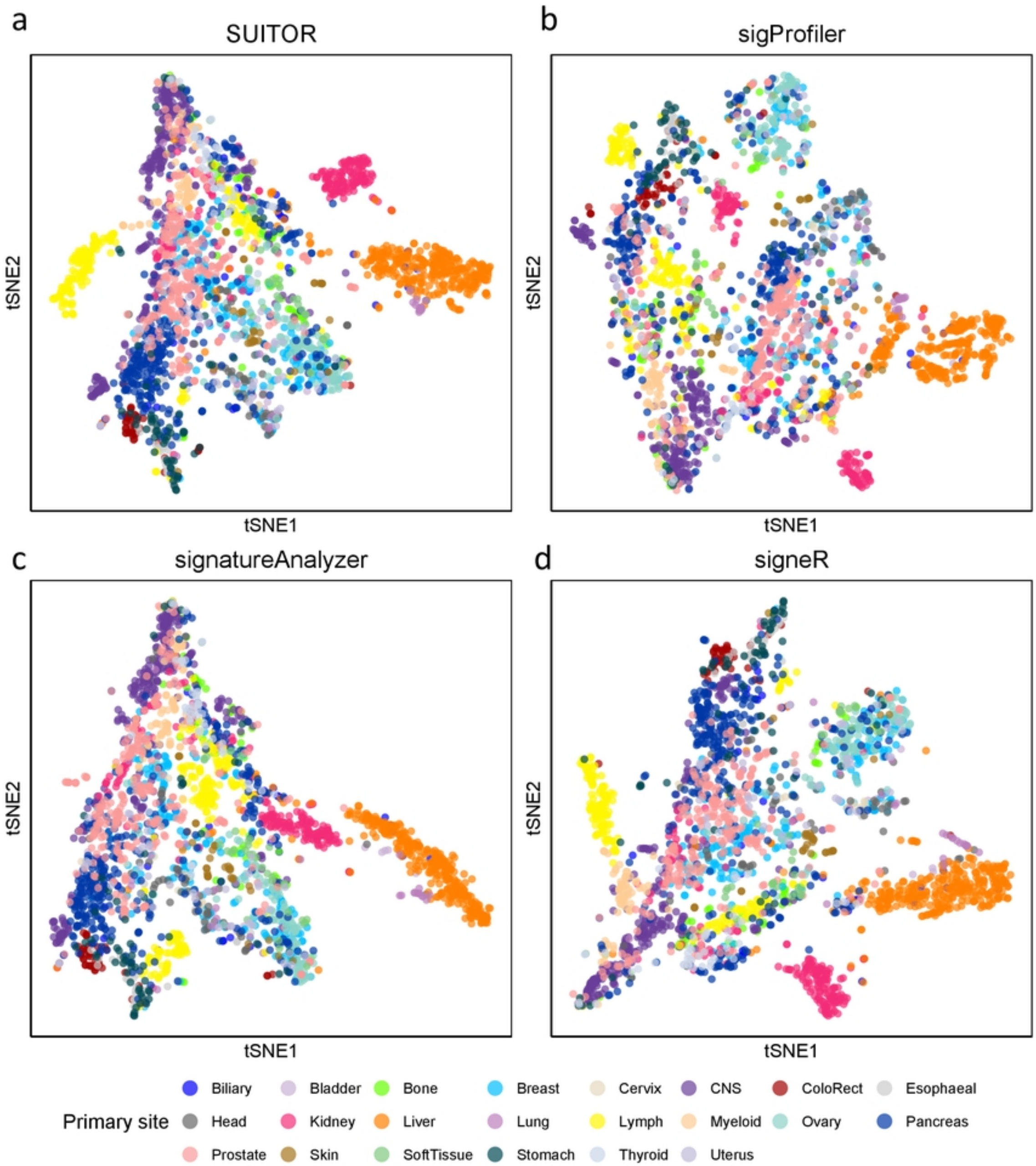
a
SUITOR
tSNE2
tSNE1
b
sigProfiler
tSNE2
tSNE1
c
signatureAnalyzer
tSNE2
tSNE1
d
signeR
tSNE2
tSNE1
Primary site
Biliary
Bladder
Bone
Breast
Cervix
CNS
ColoRect
Esophaeal
Head
Kidney
Liver
Lung
Lymph
Myeloid
Ovary
Pancreas
Prostate
Skin
SoftTissue
Stomach
Thyroid
Uterus

Figure 6

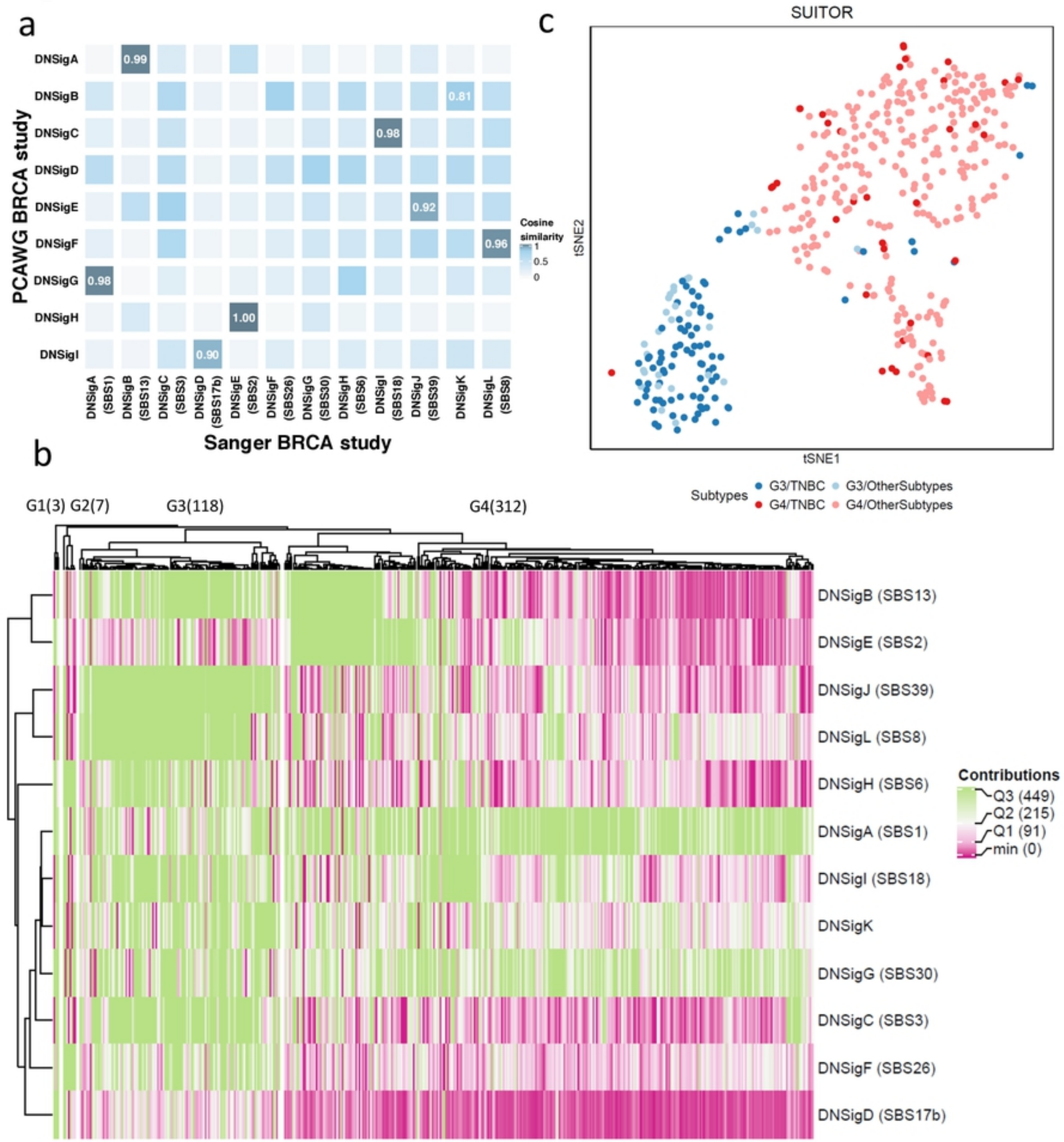
a
PCAWG BRCA study
Sanger BRCA study
DNSigA
DNSigB
DNSigC
DNSigD
DNSigE
DNSigF
DNSigG
DNSigH
DNSigI
DNSigA (SBS1)
DNSigB (SBS13)
DNSigC (SBS3)
DNSigD (SBS17b)
DNSigE (SBS2)
DNSigF (SBS26)
DNSigG (SBS30)
DNSigH (SBS6)
DNSigI (SBS18)
DNSigJ (SBS39)
DNSigK
DNSigL (SBS8)
0.99
0.81
0.98
0.92
0.96
0.98
1.00
0.90
Cosine similarity
1
0.5
0
c
SUITOR
tSNE1
tSNE2
b
G1(3) G2(7)
G3(118)
G4(312)
Subtypes
G3/TNBC
G3/OtherSubtypes
G4/TNBC
G4/OtherSubtypes
DNSigB (SBS13)
DNSigE (SBS2)
DNSigJ (SBS39)
DNSigL (SBS8)
DNSigH (SBS6)
DNSigA (SBS1)
DNSigI (SBS18)
DNSigK
DNSigG (SBS30)
DNSigC (SBS3)
DNSigF (SBS26)
DNSigD (SBS17b)
Contributions
Q3 (449)
Q2 (215)
Q1 (91)
min (0)